PROJECT REPORT

On

FABRICATION OF g-C_3N_4/$NiCo_2O_4$ HETEROSTRUCTURE FOR SUPERIOR PHOTOCATALYTIC PERFORMANCE

Submitted by

SHEREENAMOL P.S
(AB23CHE012)

In partial fulfillment for the award of the

Bachelor's Degree in Chemistry

DEPARTMENT OF CHEMISTRY AND CENTRE FOR RESEARCH

ST. TERESA'S COLLEGE (AUTONOMOUS)
ERNAKULAM

2025-2026

DEPARTMENT OF CHEMISTRY AND CENTRE FOR RESEARCH

ST. TERESA'S COLLEGE (AUTONOMOUS)

ERNAKULAM

B.Sc. CHEMISTRY PROJECT REPORT

Name	:	**SHEREENAMOL P.S**
Register Number	:	**AB23CHE012**
Year of Work	:	**2025-2026**

This is to certify that the project "FABRICATION OF g-C_3N_4/$NiCo_2O_4$ HETEROSTRUCTURE FOR SUPERIOR PHOTOCATALYTIC PERFORMANCE"is the work done by SHEREENAMOL P.S

Dr. Saritha Chandran A.
Head of the Department

Dr. Merin Joseph
Staff-member in charge

Submitted to the Examination of Bachelor's Degree in Chemistry

Date: 10/04/26

Examiners: SENJU DEVASY KUTTI

: Lenda Anto

DEPARTMENT OF CHEMISTRY AND CENTRE FOR RESEARCH

ST. TERESA'S COLLEGE (AUTONOMOUS)

ERNAKULAM

CERTIFICATE

This is to certify that the project work entitled "FABRICATION OF g-C_3N_4/$NiCo_2O_4$ HETEROSTRUCTURE FOR SUPERIOR PHOTOCATALYTIC PERFORMANCE" is the work done by SHEREENAMOL P.S under my guidance in the partial fulfillment of the award of the Degree of Bachelor of Science in Chemistry at St. Teresa's College (Autonomous), Ernakulam affiliated to Mahatma Gandhi University, Kottayam.

DR. MERIN JOSEPH
(Project Guide)
Department of Chemistry and Centre for Research
St. Teresa's College, Ernakulam

DECLARATION

I hereby declare that the project work entitled "FABRICATION OF g- $C_3N_4/NiCo_2O_4$ HETEROSTRUCTURE FOR SUPERIOR PHOTOCATALYTIC PERFORMANCE" submitted to Department of Chemistry and Centre for Research, St. Teresa's College (Autonomous) affiliated to Mahatma Gandhi University, Kottayam, is a record of an original work done by me under the guidance of **DR.MERIN JOSEPH, ASSOCIATE PROFESSOR ,** Department of Chemistry and Centre for Research, St. Teresa's College (Autonomous), Ernakulam and this project work is submitted in the partial fulfillment of the requirements for the award of the Degree of Bachelor of Science in Chemistry.

SHEREENAMOL P.S

Acknowledgements

We would like to express our deepest gratitude to those who have contributed significantly to the completion of this project work. First and foremost, we would like to acknowledge the divine guidance and blessings that have enabled us to complete this project. We would like to thank our research guide, Dr. Merin Joseph, Assistant Professor Department of Chemistry, St. Teresa's College (Autonomous), Ernakulam for her invaluable guidance, Support, and encouragement throughout this project. We extent our sincere gratitude to Rev.Sr. Nilima CSST, Manager; and the Directors, Rev. Sr. Francis Ann CSST and Rev. Sr. Tessa CSST, St. Teresa's College (Autonomous), Ernakulam, Dr. Anu Joseph, Principal, Dr. Saritha Chandran A, Head of the Department, and all the faculty members of the Department of Chemistry, St. Teresa's college (Autonomous), Ernakulam for providing us the infrastructure required for this project and their well wishes. We would also like to extend our heartfelt thanks to all the non-teaching staffs of the Department of Chemistry, St. Teresa's College, Ernakulam for their assistance and support during the experimental work. To our family and friends, We are forever grateful for their unwavering support, love, and sacrifices throughout this journey. Thank you once again to everyone who has made this project possible.

SHEREENAMOL P.S

Contents

Chapter 1

Introduction

The concern over environmental degradation and the need for clean, sustainable energy has grown on a global scale and has drawn attention from the nanoscience community, environmentalists, legislators, economics, and many other parties [1]. This is the result of rapid depletion of energy sources such as fossil fuels, which are not environment friendly [2]. Photocatalysts based on metals, such as platinum, cadmium sulfide, and titanium dioxide are lethal for the environment. In order to address these issues, solar energy conversion provides a clean, and sustainable alternative. Therefore, there is a search for eco-friendly and green nanostructured materials that can drive photo-initiated reactions for synthesis and environmental cleanup as well as store solar energy and transform it into useful forms, such electricity [3]. Over the preceding decade polymeric graphitic carbon nitrides is one such material that has captivated considerable attention within diverse scientific domains [4]. Graphitic carbon nitride has a long history, dating back to 1834 when Berzelius synthesized a polymeric derivative and it was named as "melon" by Liebig is shown in figure 1. It is presumably one of the oldest reported polymers in the scientific literature. However, its inherent potential remained largely latent until contemporary times due to its chemical inertness, insolubility in various solvents, and an enigmatic structure [5].

Elemental analysis was conducted for the first characterization of carbon nitride (C_3N_4) compounds due to their high purity. However, all compounds were not well developed and could not establish a reproducible chemical formula. Franklin studied and reinvestigated the compounds which led to the discovery that carbonic nitride $(C_3N_4)x$ could be the final polymerization product of heating melon. However, the real evidence was still ambiguous. In 1937, Pauling and Sturdivant suggested a coplanar tri-s-triazine unit as the essential structural motif of various polymeric derivatives. Three years later, Redemann and Lucas discovered a formal resemblance between graphite and melon, and inferred that 2,5,8-triamino-tris-s-triazine ($C_{126}H_{21}N_{175}$) best described Franklin's C_3N_4. They concluded that a single crystal structure should not be assigned to melon due to its combination of various architectures and sizes [6]. In 1972, Fujishima and Honda observed water splitting on TiO_2 when exposed to UV light. After that researcher evaluated the photocatalytic performance of broad-spectrum semiconductor materials [7]. In 1982, Leonard and co-workers reported the first crystal structure of a cyameluric derivative, confirming Pauling's structure proposed 45 years ago [8]. In 2009, Wang et al. found that g-C_3N_4 has photocatalytic properties under visible light which led to the recognition of its true potential for membrane modification since then more studies have been followed in this field [9].

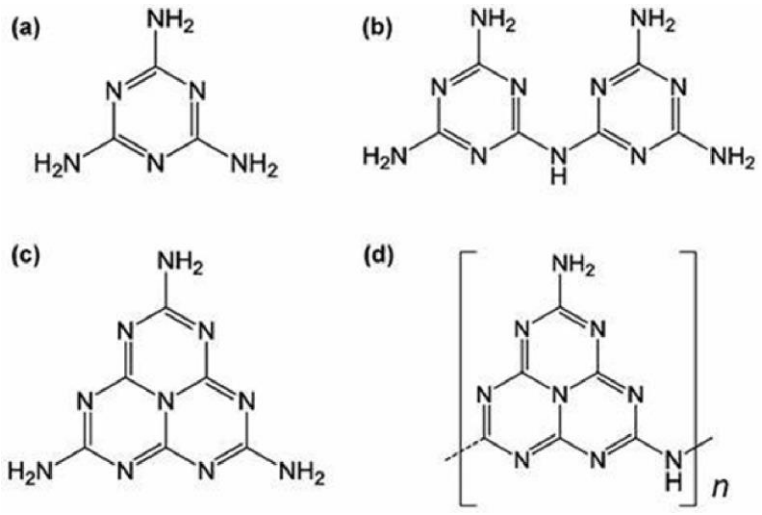

Fig 1. ***Carbon- and nitrogen-containing materials obtained from the thermolysis of mercury(II) thiocyanate as described by Liebig a) melamine b) melam c) melem and d) melon***

Graphitic carbon nitride (g-C_3N_4) is a layered material made of π-conjugated graphitic planes formed by sp^2-hybridized carbon and nitrogen atoms. Its structure is mainly built from triazine (C_3N_3) and tri-s-triazine (C_6N_7) units, with the latter being more stable. Unlike graphene's honeycomb structure, g-C_3N_4 contains uniformly distributed triangular nanopores. It is the most stable allotrope of carbon nitride under ambient conditions, is insoluble in most solvents, thermally stable up to about 600 °C in air, has a layer spacing of ~0.326 nm, and shows low electrical conductivity (<1 S cm^{-1})[1].

g-C_3N_4 has the highest nitrogen content among carbon-based 2D materials and remains stable in acidic and alkaline environments. Its bonding involves sp^2-hybridized carbon and nitrogen atoms arranged in conjugated networks, with weak intermolecular interactions such as hydrogen bonding and van der Waals forces between layers. The π-conjugated structure gives g-C_3N_4

a moderate band gap. Because of its chemical inertness and unclear structure, it was not widely explored until recent years [1]. As a metal-free n-type polymeric semiconductor, g-C_3N_4 exhibits promising electrical, optical, and physicochemical properties, making it useful in electronic, catalytic, and energy applications. Since the first report of photocatalytic H_2 and O_2 evolution in 2009, interest in g-C_3N_4-based photocatalysts has rapidly increased. These materials are now widely studied for water splitting, pollutant degradation, and CO_2 reduction, and are becoming important alternatives to graphene-based photocatalysts in energy and environmental fields [8].

As a metal-free semiconductor, g-C_3N_4 can be easily modified to form hybrid photocatalysts with controllable size, thickness, porosity, and morphology. Various nanostructures such as 1D nanorods, 2D nanosheets, and 3D hierarchical structures have been developed to improve solar light absorption, charge separation, and surface reactivity. Although many reviews focus on synthesis and modification, fewer discuss the versatile properties and rational design of g-C_3N_4-based photocatalysts. Therefore, continued research is important for improving solar energy utilization and expanding applications in sustainable energy devices such as solar cells, fuel cells, batteries, and sensors [8].

Due to the depletion of fossil fuels and their environmental impact, hydrogen is considered a clean alternative energy source. Photocatalytic hydrogen production is especially attractive because it can occur under ambient conditions using solar energy, similar to natural photosynthesis [4]. g-C_3N_4 has gained attention for this purpose because of its unique electronic structure. The lone pair electrons on nitrogen form the valence band, while

carbon atoms mainly contribute to the conduction band. This band structure allows effective separation of photogenerated electrons and holes. With a band gap of about 2.7 eV, g-C_3N_4 can absorb visible light and is suitable for water purification, hydrogen generation, and solar energy applications [3].

1.1 Structure of g-C_3N_4

Graphitic carbon nitride (g-C_3N_4) is a two-dimensional polymeric material made entirely of sp^2-hybridized carbon and nitrogen atoms linked by strong covalent bonds. Because carbon and nitrogen can form different bonding arrangements, g-C_3N_4 shows some structural variations, including defect and amorphous forms. However, the graphitic form is the most stable under normal conditions. Its structure, composition, and crystallinity are commonly studied using techniques such as XRD, XPS, and Raman spectroscopy. Early studies on carbon nitride compounds began in the 19th century, and later research confirmed the existence of graphitic C_3N_4 structures. The material has a graphite-like layered framework where nitrogen atoms substitute some carbon atoms, leading to π-conjugated planes with strong in-plane bonding and weak van der Waals forces between layers. This nitrogen incorporation slightly changes the interlayer distance compared to graphite and influences the electronic structure of g-C_3N_4 [2].

g-C_3N_4 is a π-conjugated polymeric n-type semiconductor composed mainly of carbon and nitrogen. It is the most stable allotrope of carbon nitride at ambient conditions and has unique surface properties such as basic functional groups, electron-rich nature, and hydrogen-bonding ability, which are useful in photocatalysis. Structurally, it consists of repeating

triazine or tri-s-triazine units arranged in layered sheets similar to graphite.g-C_3N_4 can be synthesized from inexpensive nitrogen-rich precursors like melamine, urea, thiourea, and dicyandiamide using methods such as thermal polycondensation, solvothermal synthesis, microwave irradiation, and self-assembly techniques. Preparation conditions and precursor types strongly affect its optical and structural properties; for example, urea-derived g-C_3N_4 may show a slightly larger band gap than thiourea-derived samples. These tunable properties make g-C_3N_4-based materials suitable for various multifunctional applications, especially in photocatalysis [4].

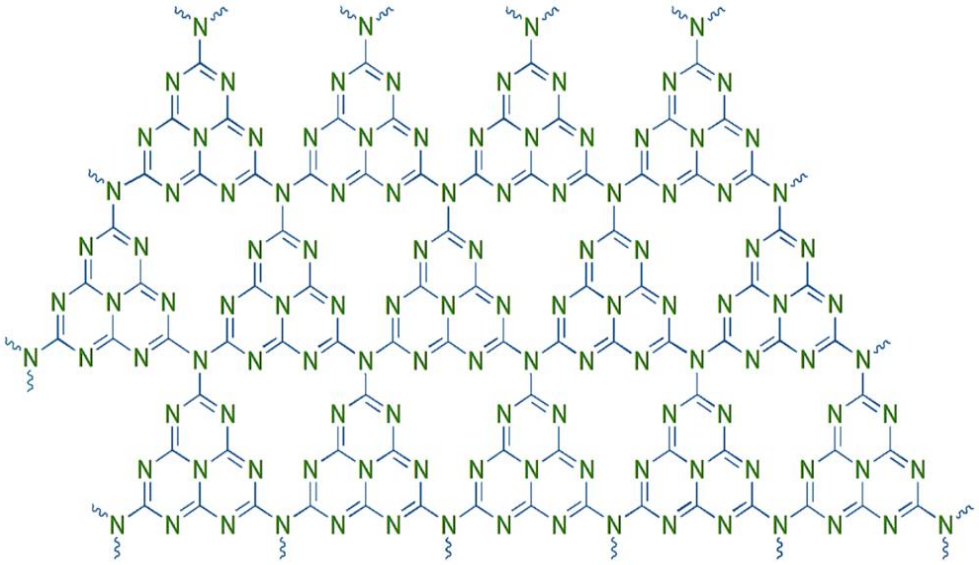

Fig 2. represents the structure of g-C_3N_4

Such as band gap and light absorption are usually studied using UV–Vis and photoluminescence techniques. Structural modifications and nanostructuring (e.g., mesoporous forms) can improve light harvesting, charge separation, and electrical conductivity, enhancing photocatalytic performance [3].

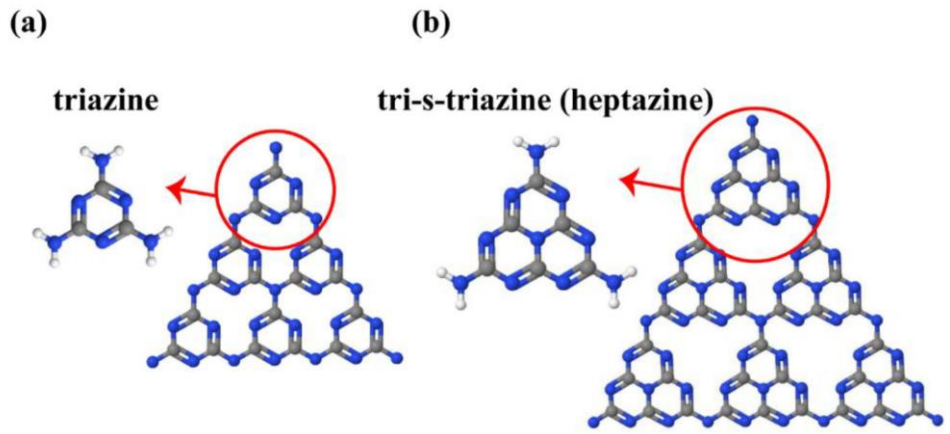

Fig 3. a) Tri-s-triazine and 3b) triazine structures of g-C_3N_4

Unlike metal-based photocatalysts, g-C_3N_4 is metal-free and non-toxic, avoiding problems such as metal leaching and photocorrosion. Its suitable band structure allows visible-light absorption and generation of electron–hole pairs, making it an environmentally friendly material for sustainable photocatalysis [10]. Two-dimensional g-C_3N_4 nanosheets have much higher surface area (50–400 $m^2\ g^{-1}$) than bulk g-C_3N_4 (<10 $m^2\ g^{-1}$). Their thin structure shortens charge migration distance and improves in-plane conductivity. Their large surface area and abundant active sites enhance light absorption, mass transport, and photocatalytic activities [1]. The properties of g-C_3N_4 can be tuned by modifying nitrogen-rich precursors before synthesis. Acid treatments (e.g., H_2SO_4 or HCl) increase surface area and porosity. Sulfur-assisted synthesis using thiourea or elemental sulfur creates structural defects, improves light absorption, and narrows the band gap. These modifications enhance charge separation and photocatalytic efficiency [11].

1.2 Properties of g-C_3N_4

g-C_3N_4 shows excellent thermal stability compared to many organic polymers. TGA studies reveal slow decomposition below 600 °C and complete decomposition near 750 °C. Stability varies slightly with precursor and preparation method. This high thermal resistance allows the g-C_3N_4 to function in high-temperature catalytic processes and also makes it useful as a template or nitrogen source for synthesizing other advanced materials [11]. The electronic structure of g-C_3N_4 is governed by nitrogen lone pair electrons, which form the valence band, while carbon contributes mainly to the conduction band. Its band gap (~2.6–2.7 eV) enables visible-light absorption. Theoretical and experimental studies show that charge separation occurs at carbon and nitrogen sites, supporting redox reactions. Doping and structural modification can tune the band structure and improve photocatalytic performance [3]. g-C_3N_4 is chemically stable and insoluble in water, acids, bases, and most organic solvents. It remains stable in air for long periods and shows strong resistance to chemical attack, though strong oxidants or molten alkalis can degrade it. Its excellent thermal and chemical stability make it useful as a catalyst, template, or precursor for other nanomaterials. Protonation in strong acids can exfoliate it into nanosheets without destroying its structure [3].

g-C_3N_4 absorbs visible light with a typical band gap of ~2.7 eV. Increasing polymerization or doping with elements such as Fe, S, P, or B can shift the absorption edge toward longer wavelengths. It exhibits strong blue photoluminescence (~470 nm), related to band gap emission. Lower PL intensity generally indicates better charge separation and higher photocatalytic activity. g-C_3N_4 also shows electrochemiluminescence, making it useful in sensing and optoelectronic applications [3]. g-C_3N_4 absorbs visible light with a typical band gap of ~2.7 eV. Increasing

polymerization or doping with elements such as Fe, S, P, or B can shift the absorption edge toward longer wavelengths. It exhibits strong blue photoluminescence (~470 nm), related to band gap emission. Lower PL intensity generally indicates better charge separation and higher photocatalytic activity. g-C_3N_4 also shows electrochemiluminescence, making it useful in sensing and optoelectronic applications [3].

Precursors	Temperature (in°C)	Band Gap (eV)	Application
Urea	450-550	2.7	Water splitting
Thiourea	450-650	2.4-2.6	Organic Pollutant Degradation
Dicyandiamide	450-550 >600 (Collapse)	2.7-2.8	Bacterial Inactivation
Cyanamide	550	2.7-2.8	Photoelectrochemical devices
Dicyandiamide under H_2	450-550	2.5-2.6	Hydrogen Production
Cyanamide under CO_2	500-580	2.4-2.5	CO_2 photoreduction to fuels (CH_4,CO)
Melamine	500-580	2.8-3.0	Fluorescent sensors[14]

Table. 1 Synthesis Parameters, Properties and Applications of g-C_3N_4

1.3 Synthesis of g-C_3N_4

Graphitic carbon nitride (g-C_3N_4) is commonly synthesized by thermal polymerization of nitrogen-rich precursors such as melamine, urea, thiourea, cyanamide, and dicyandiamide. The process involves two temperature-dependent steps: polyaddition, where precursors form melamine-based intermediates, and polycondensation, where ammonia is released to form the final g-C_3N_4 polymer. The choice of precursor and calcination temperature strongly influence surface area, porosity, band gap, and nanostructure. Characterization is typically carried out using XRD,

FTIR, XPS, and UV–Vis DRS, while DFT studies show that the valence and conduction bands mainly arise from nitrogen and carbon p-orbitals [12]. Higher calcination temperatures generally improve polymerization, increase the C/N ratio, enhance π-conjugation, and shift light absorption toward longer wavelengths, giving darker-colored samples with better visible-light activity. However, incomplete condensation at low temperatures can introduce excessive defects that hinder charge transport. Thiourea- and urea-derived g-C_3N_4 are widely studied because they can produce porous nanosheet structures without templates. During urea polymerization, released gases such as NH_3 and CO_2 act as self-templates, forming nanoporous structures with high surface area and improved photocatalytic hydrogen production [12].

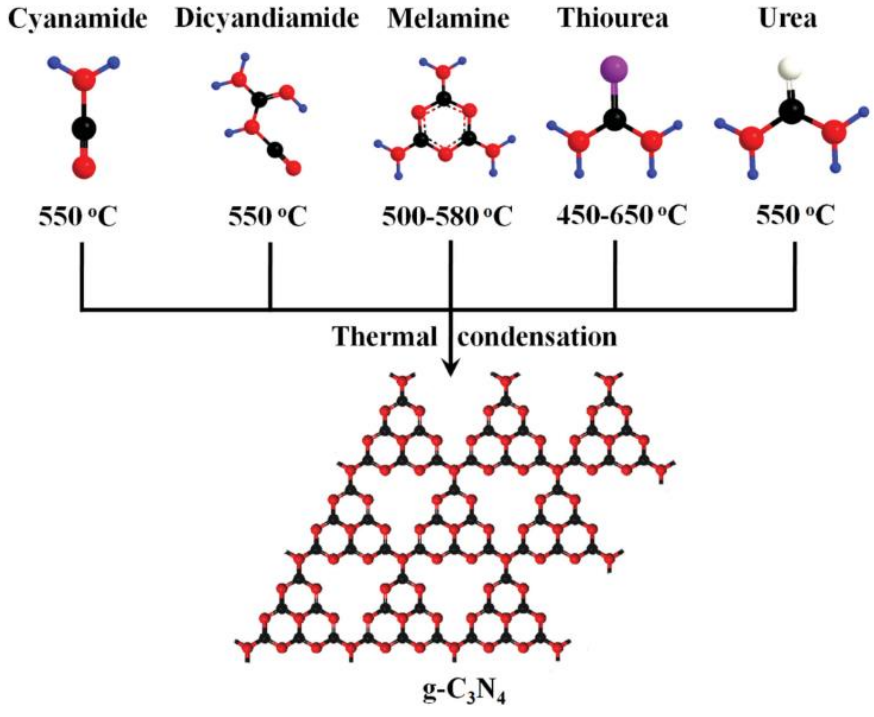

Fig 4. Schematic illustration of the main synthesis routes of bulk g-C_3N_4

1.4 Modifications of g-C_3N_4

g-C_3N_4 has demonstrated excellent photocatalytic activity due to its appropriate band gap energy and ability to absorb light within the visible range of solar spectrum. The material's polymeric nature is another significant aspect that supports its application in environmental remediation from hazardous inorganic and organic chemicals or in water splitting to generate hydrogen [13]. Even though g-C_3N_4 has a suitable bandgap and higher stability towards photocatalytic reactions, its photocatalytic activity is still below expectations. In order to improve the efficiency, efforts should be made to increase electron-hole pairs also enhance charge carrier separation and migration, and induce active sites on photocatalyst surfaces. g-C_3N_4-based materials can be prepared using multiple strategies to modulate electronic structure and intrinsic physiochemical properties. Modifications include elemental doping, defect engineering, and morphology modulation. Additionally, g-C_3N_4 composites can be constructed using cocatalyst loading, heterojunctions, and multi-component systems, enhancing photocatalytic efficiency [14].

1.4.1 Structural modification

Photocatalytic efficiency depends strongly on precursor choice, porosity, and supramolecular assembly. These factors influence band gap, morphology, and charge transport [15]. Creating porosity increases surface area, improves mass transfer, and reduces electron–hole recombination. Hard templates (like silica) and soft templates (gas bubbles or surfactants) are widely used. Porous g-C_3N_4 shows significantly improved antibiotic degradation under visible light. However, some hard-template methods are costly and less suitable for large-scale use[15].

1.4.2 Elemental doping

Doping in semiconductor photocatalyst is generally a band engineering strategy by virtue of which the bandgap reduction and extended absorption towards the visible region of the solar spectrum occur. In the case of g-C_3N_4 lattices, thereby resulting in substitutional or interstitial doping [15]. Metal doping generally takes place by the insertion of metal atoms into the g-C_3N_4 framework via cave doping, in which metal atoms get fixed into the large nitride pores (pots) of triazine units by the strong electrostatic attraction between negatively charged nitrogen and the positive metal cations. The reduction in bandgap is achieved via the introduction of additional energy levels by metallic impurities, which may be lower or higher than the CB minimum and VB maximum, respectively, to reduce the bandgap values. Many alkali/alkaline earth metals, transition metals or noble metals are incorporated into the g-C_3N_4 matrix by adding soluble salts during thermal condensation polymerisation. Metal incorporated g-C_3N_4 for antibiotic removal is systematically done[15]. Cave doping alkali metal cation induces non-uniform spatial charge distribution in different directions and thereby enhance charge transfer kinetics and an increased number of charge carriers. A systematic study on the effect of different alkali and alkaline earth metals (Na, K, Ca, Mg) on the textural properties of urea derived g-C_3N_4 and its application in photocatalytic degradation of enrofloxacin was reported by Yan et al.. The XPS, TEM, and FTIR measurements revealed the incorporation of urea's oxygen atom into the g-C_3N_4 matrix during metal incorporation. The combined effect of dopants and structural oxygen atoms strongly influences the material's morphology and band structure. Besides, there is a reduction in the doped system's surface area values due to the agglomeration of doped g-C_3N_4 and limited CO_2 release during thermal condensation. In a similar study Ba ion doping into g-C_3N_4 for the

degradation of TC was reported with decreased bandgap and increased photocarrier generation. The TC degradation intermediates were identified by liquid chromatography-mass spectrometry (LC-MS). In the latest report, Yan et al. demonstrated the use of K doped g-C_3N_4 for the degradation of enrofloxacin using a modified Fenton process. Also, structural oxygen was incorporated into the triazine moieties, which helped to improve the photocatalytic degradation performance[15]. Form Schottky junctions and exhibit surface plasmon resonance (SPR), enhancing light absorption and reducing recombination. Useful for simultaneous hydrogen production and antibiotic degradation[15].

Non-metals (O, S, P, B, F, Cl, Br, I, C, N) substitute into the lattice, improving conductivity, creating vacancies, and extending visible-light absorption.Its examples include Carbon or nitrogen doping for better charge separation,Sulfur or phosphorus doping for bandgap tuning,Halogen doping (Cl, Br) for nanosheet formation and higher surface area.Non-metal doping is cost-effective and thermally stable but requires controlled concentrations to avoid recombination losses [15].

Co-doping combines advantages of both dopant types, improving electrical conductivity, surface area, and charge separation simultaneously. Systems such as C–Ce, S–Gd, K–I, Ag–P doped g-C_3N_4 show much higher antibiotic degradation efficiency than single-doped or pristine materials. However, precise control of dopant position and concentration is essential for best performance [15].

1.5 Heterojunction Formation

Photocatalysis is limited in practical applications due to the low quantum efficiency of catalysts in utilizing solar energy. The rapid recombination of photogenerated electrons and holes is a major cause of poor photocatalytic

performance. Forming semiconductor heterojunctions by coupling two photocatalysts with suitable valence band (VB) and conduction band (CB) positions is an effective strategy to improve charge separation and transfer [16]. Various g-C_3N_4-based heterojunctions have been developed for environmental remediation and energy conversion. TiO_2 is widely used to form heterostructures with g-C_3N_4, significantly enhancing photocatalytic activity. Coupling g-C_3N_4 with materials such as Cu_2O, Ni complexes, graphene, red phosphorus, TiO_2, CdS, and others improves light absorption, charge separation, and hydrogen evolution reaction (HER) performance [16]. Beyond conventional semiconductors, g-C_3N_4 has also been combined with metal–organic frameworks (MOFs) like UiO-66. MOFs are porous crystalline materials made of metal ions and organic linkers, known for high surface area and tunable properties. When integrated with g-C_3N_4, UiO-66 enhances charge transport and suppresses recombination, leading to improved photocatalytic degradation efficiency. The strong interfacial contact between UiO-66 and g-C_3N_4 is responsible for this enhancement [16].

In photocatalysis, catalysts generate electrons and holes that drive surface redox reactions. Enhancing light absorption at longer wavelengths increases the number of charge carriers available. An ideal photocatalyst has a band gap near 2.0 eV, while g-C_3N_4 has a wider 2.7 eV band gap with absorption up to 460 nm. Doping with metal and non-metal heteroatoms narrows the band gap and extends light absorption[16].

Various alloying elements such as Ti, Cr, Fe, Ni, Cu, Zn, and Mn have been incorporated into carbon-based frameworks to form metal–polymer–carbon composites. Similar strategies produced N-doped bimetal catalysts like FeCo-MCN-900 with excellent electrocatalytic properties. In g-C_3N_4, doped heteroatoms are often distributed on surface layers, broadening the

absorption spectrum and improving photocatalytic performance under solar light. Heteroatom coupling can extend light absorption of g-C_3N_4 beyond 650 nm, improving visible-light utilization. This is particularly beneficial for photocatalytic bacterial disinfection. Traditional disinfection methods like chlorination and ozonation produce harmful by-products, while UV treatment often allows bacterial regrowth. Solar-driven photocatalytic disinfection offers a safer alternative [16].

1.6 Nickel Cobaltite ($NiCo_2O_4$)

$NiCo_2O_4$ (Nickel Cobaltite) is a mixed transition metal oxide that crystallizes in a spinel structure (AB_2O_4), where both nickel and cobalt cations occupy the tetrahedral and octahedral sites, respectively. In this compound, Ni^{2+} ions typically occupy tetrahedral positions, while Co^{3+} and Co^{2+} ions are distributed within octahedral sites, forming either a normal or inverse spinel configuration. The coexistence of multiple oxidation states (Ni^{2+}/Ni^{3+} and Co^{2+}/Co^{3+}) contributes to its enhanced electrical conductivity, which arises from efficient electron hopping between metal centers. $NiCo_2O_4$ also exhibits excellent thermal and chemical stability, ensuring reliable performance under harsh operational conditions.

The magnetic behaviour of $NiCo_2O_4$ is attributed to the strong electronic interactions between transition metal ions, which result in distinctive magnetic properties. The compound can be synthesized using various synthetic routes, including hydrothermal, sol–gel, co-precipitation, solid-state reaction, and combustion methods, allowing control over its morphology and particle size. Due to its outstanding physicochemical properties, $NiCo_2O_4$ has gained significant attention in a wide range of applications. It serves as an efficient electrocatalyst for the oxygen evolution reaction (OER) and is widely employed in supercapacitors and

lithium-ion batteries owing to its high electrical conductivity and redox activity. Additionally, its photocatalytic efficiency enables effective dye degradation and environmental remediation, while its magnetic and sensing properties make it suitable for use in gas sensors and magnetic materials.

One of the key advantages of $NiCo_2O_4$ is its superior electrical conductivity compared to individual oxides such as NiO and Co_3O_4. Moreover, it possesses a narrow bandgap energy (approximately 1.6–2.4 eV, depending on synthesis conditions), which enhances its visible-light photocatalytic activity. The combination of its structural versatility, electronic conductivity, thermal stability, and catalytic functionality establishes $NiCo_2O_4$ as a promising multifunctional material for advanced energy conversion, storage, and environmental applications. The material usually exhibits a high surface area and mesoporous structure with pore sizes around 9 to 10 nanometres, which promote electroactive sites for catalytic reactions and facilitate ion diffusion. Advanced characterizations such as X-ray diffraction confirm the high crystallinity and phase purity of $NiCo_2O_4$, and spectroscopic analyses like Raman and FTIR demonstrate metal-oxygen bonding in the spinel lattice that is critical for its catalytic and electrochemical activity. These electronic and structural attributes contribute to enhanced conductivity, cycling stability, and overall improved performance in applications such as supercapacitors, batteries, photocatalysis, and electrochemical sensors. In particular, the synergy between Ni and Co ions enhances charge transfer kinetics and catalytic activity in oxygen and hydrogen evolution reactions, positioning $NiCo_2O_4$ as a promising multifunctional material [4].

1.7 Antibiotic Degradation

Ciprofloxacin (CIP) is one of the fluoroquinolones that make up nearly 17% of the worldwide pharmaceutical market [17]. Despite its extensive antibacterial action, CIP is a second-generation antibiotic that is not completely degradable. A living organism excretes more than 75% of CIP, which finds its way into municipal wastewater and causes bacterial antibiotic resistance as well as biotoxicity in some probiotics. Titanium dioxide (TiO_2) is a common choice for photocatalysis because of its outstanding photocatalytic efficacy, low cost, high stability, and non-toxicity. Photocatalysis is a promising way to remove CIP from water. However, because of its large band gap, TiO_2 has a lower sensitivity to visible light and facilitates the simple recombination of photogenerated electron-hole pairs [18]. In order to prevent the recombination of electron-hole pairs, composite catalysts with the appropriate bands have been created. Recently the TiO_2/g-C_3N_4 composite has demonstrated a wide response range to visible light and an improved separation of photogenerated electrons and holes, indicating significant potential for photocatalytic destruction of organic pollutants [19]. g-C_3N_4/TiO_2 composites have been created using a number of techniques to aid in the photodegradation of several contaminants, including phenol, propylene, norfloxacin, and Rhodamine B. According to recent research, the TiO_2/g-C_3N_4 photocatalyst offers photogenerated charge carriers a considerably freer path, enough channels, and a short diffusion distance. It is difficult to design Z-scheme composites that effectively remove CIP, but creating various morphologies is another tactic to maximize catalytic activity. Because of their distinct one-dimensional structure, TiO_2 microspheres

made of TiO_2 nanorods have demonstrated improved photocatalytic performance [19].

1.8 Objectives

- Synthesis and optimization of graphitic carbon nitrite(g-C_3N_4) from urea and thiourea precursors.
- Synthesis of $NiCo_2O_4$ spinel type cobaltates.
- Fabrication and characterization of g-C_3N_4/$NiCo_2O_4$ cobaltate heterostructure.
- Evaluation of Photocatalytic performance using Ciprofloxacin (Antibiotic) degradation.[20]

Chapter 2

Materials and Methods

This chapter gives a brief description of the materials and experimental procedures adopted for the present investigation.

2.1 Materials Required

- Urea
- Thiourea
- Nickel Nitrate
- Cobalt Nitrate
- Sodium Hydroxide
- Distilled water

2.2 Apparatus Required

- Silica crucible
- Magnetic Stirrer
- Muffle furnace
- UV-Vis lamp

2.3 Experimental Procedures

2.3.1 Preparation of g-C_3N_4

The graphitic carbon nitride samples were synthesized via a direct thermal polycondensation method using urea and thiourea as precursors. In a typical synthesis, 10 g of the precursor (urea, thiourea, and a 1:1 mass ratio mixture of both - hereafter denoted as CNU, CNT and g-CN respectively) was placed in a covered silica crucible separately. The crucible was heated in a muffle furnace in a Temperature of 500°C - 550°C. The sample was calcined at this temperature for 1 hour in an air atmosphere. After the heating process, the furnace was allowed to cool naturally to room temperature. The resulting product, obtained as a pale-yellow solid, was collected and ground into a fine powder for further physicochemical characterization [21].

2.3.2 Synthesis of $NiCo_2O_4$

The Spinel shaped Nickel cobaltite (NCO) can be synthesized using a co-precipitation - 550°C annealing method. In the first step, 3 mmol of nickel nitrate and 6 mmol of Cobalt nitrate were dissolved in 25 mL of deionized water. Simultaneously, 22.5 mmol of NaOH was dissolved in another 25 mL of deionized water. The two solutions were then mixed under stirring. The mixture was stirred in a water bath at 60°C for 30 minutes and then aged at room temperature for 2 hours. In the second step, the reaction mixture was centrifuged at high speed to obtain the solid product, which was then washed and centrifuged multiple times. In the third step, the purified solid product was placed in a tube furnace and annealed at 550°C for 3 hours in an air atmosphere, with a heating rate of 5°C per minute, to obtain the $NiCo_2O_4$ solid powder [22].

2.3.3 Preparation of $NiCo_2O_4$/g-C_3N_4 (g-CN/NCO) Hybrid Composites - Impregnation Method

An impregnation strategy was adopted for the preparation g-C_3N_4/$NiCo_2O_4$ hybrids. In a typical process, 0.5 g g-C_3N_4 was dispersed in ethanol via stirring. An ethanolic solution of $NiCo_2O_4$ was added to the above solution and further stirred for 12 hours followed by solvent evaporation under continuous stirring and heating. The samples were dried at 80˚ C for 8 hours. A g-C_3N_4/$NiCo_2O_4$ hybrids with 5 weight percentage of $NiCo_2O_4$ was synthesized and denoted hereafter as g-CN/NCO [23].

2.4 Photocatalytic Studies

The photocatalytic activity under visible light irradiation of the as-prepared g-C_3N_4 samples from different precursors was assessed using the photocatalytic degradation of methylene blue [24]. The percentage degradation of methylene blue was assessed by monitoring the absorbance of the solution at 664nm at definite time intervals.

2.5 Photocatalytic Degradation Ciprofloxacin

The application of studies of the hybrid samples were conducted. The samples were used for the degradation of the antibiotic ciprofloxacin. In a single run, 10 mg of the catalyst was dispersed in 10 ml of the aqueous solution of ciprofloxacin (10 mg/L) and the suspension was stirred in the dark to attain the adsorption/desorption equilibrium. The percentage degradation of CIP was assessed by monitoring the absorbance of the solution at 268 nm at definite time intervals [24].

2.6 Characterization Techniques

2.6.1 Fourier Transform Infrared Spectroscopy (FTIR)

FTIR spectroscopy is utilized to identify the surface functional groups and characteristic metal-ligand vibrations within the Ni-Co matrix. In mixed-metal systems, FTIR is sensitive to the chemical bonding of metal-oxygen (M–O) or metal-sulfur (M–S) groups. For example, in cobalt-nickel sulfides, a characteristic peak near 663 cm^{-1} is associated with sulfide stretching modes [25]. In oxide systems, peaks in the range of 400–700 cm^{-1} typically correspond to the stretching vibrations of Ni–O and CO–O bonds, providing evidence for the formation of a spinel lattice [26].

2.6.2 X-Ray Diffraction (XRD)

XRD is the primary tool for confirming the phase purity and crystalline structure of Ni-Co materials, such as the widely studied spinel $NiCo_2O_4$ or $NiCo_2O_4$ [27]. The diffraction pattern, representing intensity versus 2θ, allows for the identification of specific planes (e.g., JCPDS card no. 73-1702 for $NiCo_2O_4$) [26]. Shifts in peak positions relative to pure nickel or cobalt references indicate the successful integration of both metals into a single lattice [26]. Furthermore, the average crystallite size can be determined using the Scherrer equation, which is crucial for assessing the surface-to-volume ratio of the nanostructured material [27].

2.6.3 Field-Emission Scanning Electron Microscope (FESEM)

FESEM provides high-resolution imaging to examine the morphology, topography, and size distribution of Ni-Co nanostructures. These materials often exhibit complex architectures such as nanosheets, nanowires, or urchin-like microspheres [27]. The field-emission source allows for detailed visualization of these shapes at the nanoscale, which is essential because the performance of Ni-Co catalysts is heavily dependent on their morphology [28]. For instance, the inclusion of nickel as a modifier can transform simple nanoflakes into larger cubic crystals or rice-grain-shaped nanoparticles [29].

2.6.4 Ultraviolet-Visible Reflectance Spectroscopy (UV-DRS)

UV-DRS is employed to investigate the optical absorption properties and electronic band structure of solid Ni-Co compounds. This technique is particularly valuable for determining the optical bandgap (Eg) of the material using the Kubelka-Munk function. For Ni-Co sulfides, the bandgap typically ranges between 1.2 eV and 2.4 eV, depending on the synthesis method and morphology [27]. Similarly, cobalt-nickel ferrites often exhibit bandgaps between 1.6 eV and 2.1 eV, making them responsive to visible light for photocatalytic applications [27].

Chapter 3

Results and discussion

3.1 Structural, Morphological and Optical Characterization of g-C_3N_4 and g-C_3N_4/NCO

3.1.1 X-Ray Diffraction (XRD) Analysis

The X-ray diffraction patterns of pure g-C_3N_4 and g-C_3N_4/$NiCo_2O_4$ (NCO) composite are shown in Figure 5. The diffraction pattern of pristine g-C_3N_4 exhibits two characteristic peaks at $2\theta \approx 13°$ and 27.6°, corresponding to the (100) and (002) crystallographic planes, respectively. The (100) reflection arises from in-plane structural packing of tri-s-triazine units, while the strong (002) peak corresponds to interlayer stacking of conjugated aromatic layers along the c-axis direction [30,33]. The calculated interlayer distance of approximately 0.321 nm confirms the graphitic nature of the carbon nitride framework.

Upon incorporation of $NiCo_2O_4$, the composite pattern retains the prominent (002) peak of g-C_3N_4 as seen in Figure 5, indicating that the layered structure remains intact after composite formation. Spinel $NiCo_2O_4$ typically exhibits diffraction peaks corresponding to cubic crystal symmetry, as reported in literature [36]. In the present composite, the oxide peaks are either weak or slightly broadened due to low loading and fine dispersion over the two-dimensional sheets. The absence of impurity peaks confirms successful heterostructure formation without structural

collapse. Such preservation of crystallinity is essential for efficient interfacial charge transfer [31].

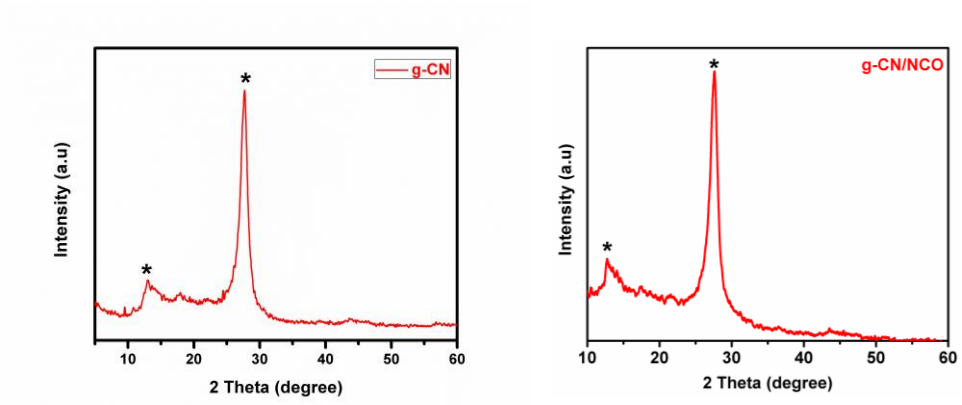

Figure 5: XRD patterns of g-C_3N_4 and g-C_3N_4/NCO composite.

3.1.2 FTIR Spectroscopic Analysis

The FTIR spectra of g-C_3N_4 and g-C_3N_4/NCO composite are presented in Figure 6. The broad absorption band in the region 3000–3500 cm^{-1} is attributed to N–H stretching vibrations of terminal amino groups and O–H stretching from adsorbed moisture. The strong peaks observed between 1200–1700 cm^{-1} correspond to stretching vibrations of aromatic C–N and C=N heterocycles, confirming the heptazine framework of g-C_3N_4 [30,34]. The distinct peak at approximately 810 cm^{-1} represents the breathing mode of tri-s-triazine units, which is considered the fingerprint of graphitic carbon nitride.

In the composite spectrum shown in Figure 6, all intrinsic peaks of g-C_3N_4 are retained, demonstrating that the polymeric backbone remains

unaffected during hybridization. Additional absorption bands appearing below 700 cm^{-1} correspond to Ni–O and Co–O stretching vibrations, confirming the successful incorporation of spinel $NiCo_2O_4$ nanoparticles [36]. The coexistence of carbon nitride vibrational features and metal–oxygen bond vibrations verifies strong chemical interaction between the two components [31].

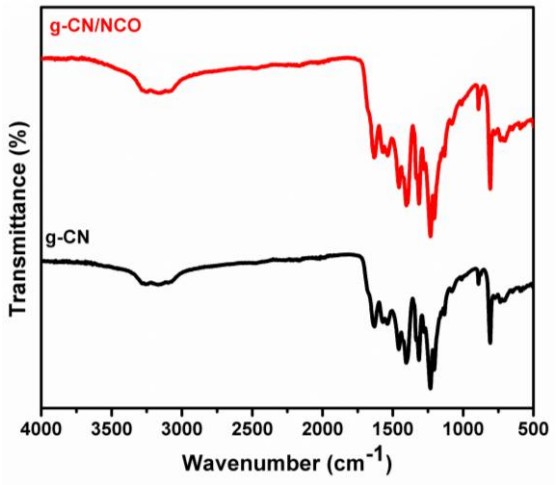

Figure 6: FTIR spectra of g-C_3N_4 and g-C_3N_4/NCO composite.

3.1.3 FE-SEM Morphological Analysis

The surface morphology of pure g-C_3N_4 and g-C_3N_4/NCO composite was investigated using FE-SEM, and the images are displayed in Figure 7. The pristine g-C_3N_4 exhibits a layered and wrinkled sheet-like morphology, characteristic of polymeric carbon nitride synthesized via thermal polymerization as shown in fig 7(a) [33]. The loosely stacked nanosheets provide high surface area and abundant adsorption sites.

After decoration with $NiCo_2O_4$ nanoparticles, the composite sample in Figure 7(b) shows uniform distribution of oxide nanoparticles over the g-C_3N_4 sheets. The surface appears rougher and more porous compared to

pure g-C_3N_4. Such intimate interfacial contact enhances electronic coupling between the semiconductors and facilitates rapid migration of photogenerated electrons across the interface, thereby suppressing recombination [31,38]. The porous structure further improves pollutant adsorption and catalytic efficiency.

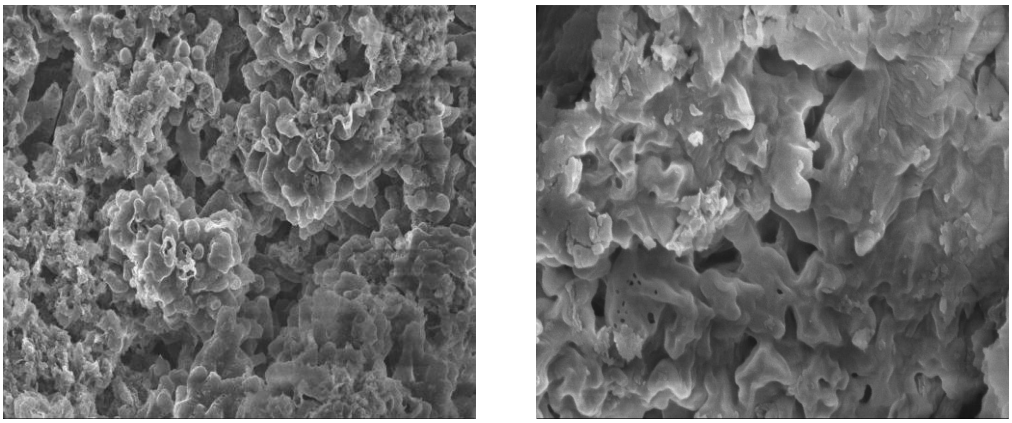

Figure 7: FE-SEM images of (a) g-C_3N_4 and (b) g-C_3N_4/NCO composite.

3.1.4 UV–DRS and Band Gap Analysis

The UV–Diffuse Reflectance Spectra of CNU, CNT and g-CN are shown in Figure 8(a), while the spectrum of g-CN/NCO composite is presented in Figure 8(b). Pure g-C_3N_4 exhibits strong absorption in the UV region with moderate extension into the visible region due to its intrinsic band gap [30]. Upon incorporation of $NiCo_2O_4$, the absorption edge shifts toward longer wavelengths (red shift), indicating enhanced visible light absorption capability [31].

The band gap values calculated from Tauc plots are summarized in Table 2. The band gap decreases from 2.84 eV (CNU) to 2.72 eV (g-CN/NCO). This narrowing of band gap facilitates easier excitation of electrons under visible light irradiation and improves photocatalytic performance [35]. The modification of electronic structure arises from strong interfacial interaction between g-C_3N_4 and $NiCo_2O_4$, which alters band alignment and promotes charge carrier mobility [31].

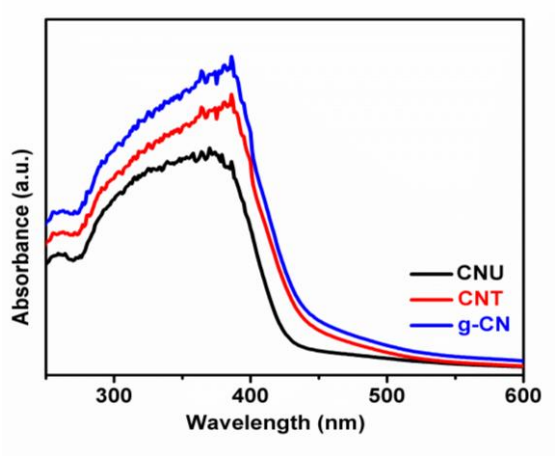

Figure 8(a): UV–DRS spectra of CNU, CNT and g-CN.

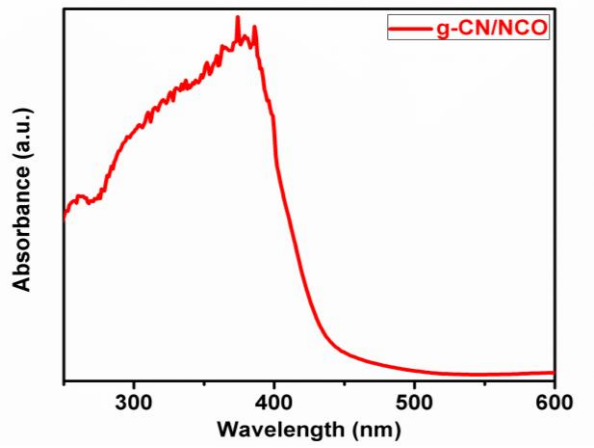

Figure 8(b): UV–DRS spectrum of g-CN/NCO composite.

Band Gap values	
CNU	2.84(eV)
CNT	2.80(eV)
g-CN	2.78(eV)
g-CN / NCO	2.72(eV)

Table 2: Band gap values of prepared samples.

3.2 Photocatalytic Studies

To optimize the combination of precursors, three different trials were conducted. Three different types of carbon nitrides were synthesized using urea, thiourea and 1:1 combination of urea and thiourea. The sample prepared with the combination of urea and thiourea named as g-CN showed maximum absorption in UV-DRS spectra. In order to further substantiate the results, the photocatalytic activity of the samples was compared. For this, the degradation of methylene blue was selected as a model reaction. In the reaction the g-CN sample exhibited pronounced activity for methylene blue degradation followed by CNT and then CNU. The reaction was conducted under visible light irradiation. The progress of the reaction was monitored using UV-Vis spectrophotometer. The concentration of methylene blue was 10 ppm. The UV profile and comparison of degradation percentages are given in figure 9.

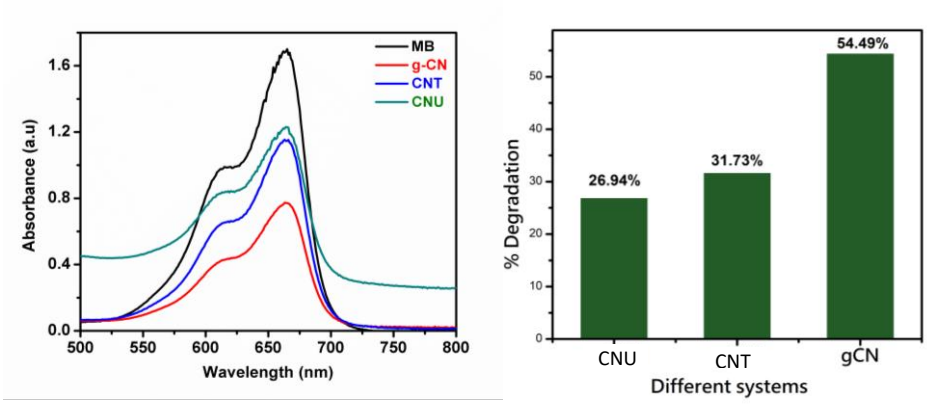

Fig.9 UV-Vis Spectra of CNU, CNT and g-CN in Degradation of Methylene Blue 9.2 Comparative Evaluation of Photocatalytic Performance.

3.3 Photocatalytic Degradation of Ciprofloxacin

The photocatalytic degradation of ciprofloxacin (CIP) under visible light irradiation was monitored using UV–Vis spectroscopy, and the absorption spectra are shown in Figure 10(a). A gradual decrease in the characteristic absorption peak intensity of CIP with increasing irradiation time confirms progressive degradation of the antibiotic molecules. Pure g-C_3N_4 exhibits approximately 55% degradation after 60 minutes.

The comparative degradation efficiencies of CNU, CNT and g-CN are presented in Figure 10(a), where g-CN shows superior activity due to its lower band gap and improved visible light absorption [30].

The degradation performance of the g-C_3N_4/NCO composite is illustrated in Figure 10(b). The composite demonstrates significantly enhanced degradation efficiency compared to pure g-C_3N_4. This improvement is attributed to efficient separation of photogenerated electron–hole pairs at the heterojunction interface [31,38]. Upon visible light irradiation, electrons migrate from the conduction band of g-C_3N_4 to $NiCo_2O_4$, while

holes remain in the valence band, thereby suppressing recombination. The accumulated electrons react with dissolved oxygen to form superoxide radicals ($O_2^{\bullet-}$), while holes generate hydroxyl radicals (•OH), which attack CIP molecules and lead to mineralization into CO_2 and H_2O [31,39].

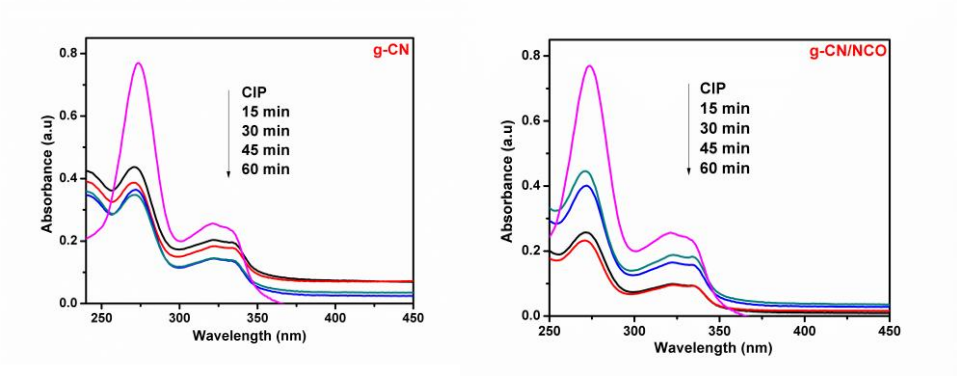

Figure 10(a): UV–Vis absorption spectra of CIP degradation using g-CN. Figure 10(b): UV–Vis absorption spectra of CIP degradation using g-CN/NCO composite

Time(min)	Absorbance	%
15	0.43	43
30	0.38	50
45	0.36	52
60	0.34	55

Time(min)	Absorbance	%
15	0.44	42
30	0.40	47
45	0.25	67
60	0.22	71

Table 3. Percentages for (a) g-CN and (b) g-CN/CCO Catalysts.

3.1 Plausible Mechanism

The improved photocatalytic performance of the $NiCo_2O_4$/g-C_3N_4 system is mainly attributed to the formation of an efficient heterojunction between $NiCo_2O_4$ and g-C_3N_4. Under simulated sunlight irradiation, both semiconductors absorb light and generate electron–hole pairs. Due to the

favourable band alignment, the photogenerated electrons in the conduction band of $NiCo_2O_4$ readily transfer to the conduction band of g-C_3N_4, while the holes in the valence band of g-C_3N_4 migrate to the valence band of $NiCo_2O_4$. This directional movement of charge carriers results in effective charge separation, with electrons accumulating on g-C_3N_4 and holes accumulating on $NiCo_2O_4$, thereby significantly suppressing electron–hole recombination. The separated charge carriers subsequently participate in redox reactions at the surface, leading to the formation of reactive oxygen species such as •OH, O_2•$^-$, and •OOH. These highly reactive species attack and degrade organic dye molecules, ultimately enhancing the overall photocatalytic efficiency of the heterostructured system.

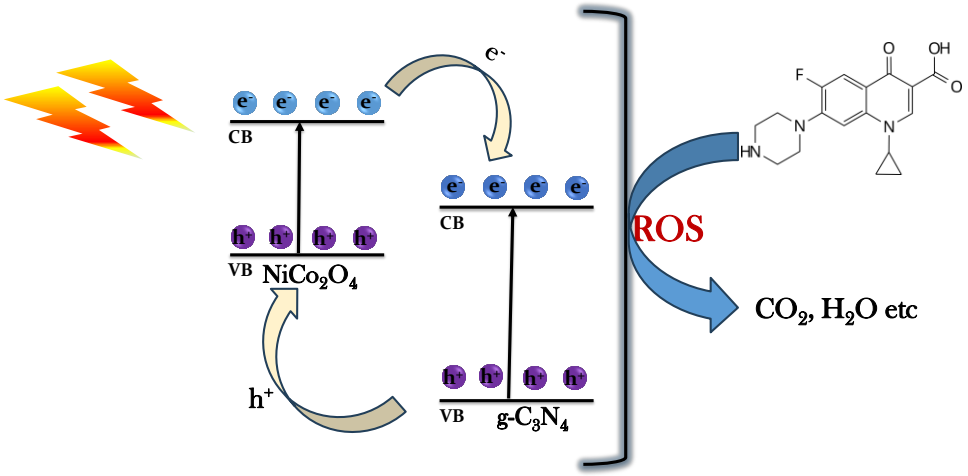

Fig.11 Schematic Representation of Plausible Mechanism: Electron Transfer Facilitating CIP Degradation.

Chapter 4

Conclusions

In this project, a g-C_3N_4/$NiCo_2O_4$ (NCO) heterostructure photocatalyst was successfully synthesized. The hybrid system was characterized using XRD, FTIR, FE-SEM and UV-DRS techniques. The structural analysis confirmed the successful formation of graphitic carbon nitride hybrid system. The XRD spectrum consists of characteristic diffraction peaks, and the incorporation of $NiCo_2O_4$ without disturbing the parent framework. FTIR results confirmed the unaltered structure of graphitic carbon nitride after impregnation. FE-SEM analysis showed layered sheet-like morphology of g-C_3N_4 and uniform distribution of NCO nanoparticles over the surface. UV–DRS studies revealed enhanced visible light absorption and a reduced band gap for the composite compared to pure g-C_3N_4. The optimization of precursors for the synthesis of graphitic carbon nitride was conducted. The precursors used were urea, thiourea and 1:1 combination of urea and thiourea. From the photocatalytic evaluation using methylene blue degradation the 1:1 combination of urea and thourea was found to be the best combination. The graphitic carbon nitride prepared from urea and thiourea were used for the development of hybrid system. The photocatalytic performance was evaluated by degradation of ciprofloxacin under visible light irradiation. The g-C_3N_4/NCO composite exhibited higher degradation efficiency compared to pure g-C_3N_4 due to improved charge separation and enhanced generation of reactive oxygen species. The results indicate that the formation of a heterojunction

between g-C_3N_4 and $NiCo_2O_4$ significantly enhances photocatalytic activity. Overall, the synthesized g-C_3N_4/NCO composite shows promising potential for visible-light-driven degradation of pharmaceutical pollutants in wastewater treatment applications.

References

1.Li, Wei, et al. "Recent progress in g–C_3N_4–Based materials for remarkable photocatalytic sustainable energy." International Journal of Hydrogen Energy 47.49 (2022): 21067.

2.Muradov, Nazim Z., and T. Nejat Veziroğlu. "“Green” path from fossil-based to hydrogen economy: an overview of carbon-neutral technologies." International journal of hydrogen energy 33.23 (2008): 6804.

3.Rono, Nicholas, et al. "A review of the current status of graphitic carbon nitride." Critical Reviews in Solid State and Materials Sciences 46.3 (2021): 189.

4.Alshammari, Alhulw H., et al. "Structural and optical characterization of g-C_3N_4 nanosheet integrated PVC/PVP polymer nanocomposites."Polymers 15.4 (2023): 871.

5.Zhu, Junjiang, et al. "Graphitic carbon nitride: synthesis, properties, and applications in catalysis." ACS applied materials & interfaces 6.19 (2014): 16449.

6.On, Wee-Jun, et al. "Graphitic carbon nitride (g-C_3N_4)-based photocatalysts for artificial photosynthesis and environmental remediation: are we a step closer to achieving sustainability?." Chemical reviews 116.12 (2016): 7159.

7.A. Fujishima and K. Honda, Electrochemical photolysis of water at a semiconductor electrode, Nature, 1972, 238(5358), 37.

8.Hosmane, R. S.; Rossman, M. A.; Leonard, N. J. Synthesis andStructure of Tri-s-Triazine.J. Am. Chem. Soc.1982,104, 5497.

9.Wen, Jiuqing, et al. "A review on g-C3N4-based photocatalysts." Applied surface science 391 (2017): 72.

10.Wang, Yong, Xinchen Wang, and Markus Antonietti. "Polymeric graphitic carbon nitride as a heterogeneous organocatalyst: from photochemistry to multipurpose catalysis to sustainable chemistry." Angewandte Chemie International Edition 51.1 (2012): 68.

11. A Targeted Review of Current Progress,Challenges and Future Perspective of g-C_3N_4 based Hybrid Photocatalyst Toward Multidimensional Applications. Asif Hayat, Muhammad Sohail, Usama Anwar, T. A. Taha, H. I. A. Qazi, Amina, Zeeshan Ajmal, Abdullah G. Al-Sehemi, Hamed Algarni, Ahmed A. Al-Ghamdi, Mohammed A. Amin, Arkom Palamanit, W. I. Nawawi,Emad F. Newair and Yasin Orooji

12. Nico2o4/g-C3N4 Heterojunction phtocatalyst for efficient H_2 production.Yanyun fan,Hongmei Chen,Danfeng Cui,Zheng Fan and Chenyang Xue

13. Ajiboye, Timothy O., Alex T. Kuvarega, and Damian C. Onwudiwe. "Graphitic carbon nitride-based catalysts and their applications: A review." Nano-Structures & Nano-Objects 24 (2020): 100577

14. Song, Xin-Lian, et al. "Engineering g-C_3N_4 based materials for advanced photocatalysis: Recent advances." Green Energy & Environment (2022).

15.Structural and compositional tuning in g-C_3N_4 based systems for photocatalytic antibiotic degradation P. Suyana, Priyanka Ganguly, Balagopal N. Nair, Suresh C. Pillai, U. S. Hareesh.

16. Highly efficient H_2 production over NiCo2 O4 decorated g-C3 N4 by photocatalytic water reduction.Wenxi Chang, Wenhua Xue, Enzhou Liu, Jun Fan, Binran Zhao

17. ojer, Carina, et al. "Clinical wastewater treatment: Photochemical removal of an anionic antibiotic (ciprofloxacin) by mesostructured high aspect ratio ZnO nanotubes."Applied Catalysis B: Environmental 204 (2017): 561.

18. Hu, Kang, et al. "Facile synthesis of Z-scheme composite of TiO2 nanorod/g-C_3N_4 nanosheet efficient for photocatalytic degradation of ciprofloxacin." Journal of cleaner production 253 (2020): 120055

19.Graphitic carbon nitride (g-C_3N_4)-based heterogeneous single atom catalysts: Synthesis, characterisation and catalytic applications. Journal of Materials Chemistry A, 2023, 11, 8599–8646.Review on SACs supported on g-C_3N_4.

20.UV–visible light sensitized NiCo2O4@g–C3N4 heterojunction: Based nanocomposites as novel photocatalysts for enhanced hydrogen generation and electrochemical activity.L. Kiran Babu, H. Seshagiri Rao, P. N. R. Kishore, N. Lakshmana Reddy, M. V. Shankar ,Y. V. Rami Reddy

21.Ezhumalai, Yamuna, et al. 'Graphite Carbon Nitride'. Photocatalysts – New Perspectives.

22.Sun, Mengxuan, et al. 'Co-Precipitation Synthesis of $CuCo_2O_4$ Nanoparticles for Supercapacitor Electrodes with Large Specific Capacity and High-Rate Capability'. Electrochimica Acta, vol. 397, Nov. 2021, p.139306.

23.Al-Aqeel, Muneerah. 'Liquid-Free Simple Synthesis of Nickel Cobaltite Nanostructures for High-Performance Supercapacitors and

Electrocatalyst Applications'. Journal of Solid-State Electrochemistry, vol. 29, no. 12, Dec. 2025, pp. 5225–32.

24.Khan, Idrees, et al. 'Review on Methylene Blue: Its Properties, Uses, Toxicity and Photodegradation'. Water, vol. 14, no. 2, Jan. 2022, p. 242.

25.Rani, P., Alegaonkar, A. P., & Alegaonkar, P. S. (2022). Evaluation of Electrochemical Performance of Cobalt Sulphide on Various Current Collectors. Material Science Research India, 19(3), 134–141.

26. Ortiz-Quiñonez, J. L., Pal, U., & Villanueva, M. S. (2018). Structural, Magnetic, and Catalytic Evaluation of Spinel Co, Ni, and Co–Ni Ferrite Nanoparticles Fabricated by Low-Temperature Solution Combustion Process. ACS Omega, 3(11), 14986–15001.

27. Ahmed, S., Ahmad, M., Yousaf, M. H., Haider, S., Imran, Z., Batool, S. S., Ahmad, I., Shahzad, M. I., & Azeem, M. (2022). Solvent-free synthesis of NiCo2S4 having the metallic nature. Frontiers in Chemistry, 10.

28. Kumar, S., Satpathy, B. K., & Pradhan, D. (2024). Morphology-controlled synthesis of a NiCo-carbonate layered double hydroxide as an electrode material for solid-state asymmetric supercapacitors. Materials Advances, 5(6), 2271–2284.

29.Ma M., et al. (2024). Recent Advances in Nickel–Cobalt-Based Materials for High-Performance Supercapacitors. Nanomaterials, 14(3), 284.

30. Wang, Y., Wang, X., & Antonietti, M. (2012). Polymeric graphitic carbon nitride as a heterogeneous organocatalyst: From photocatalysis to multifunctional catalysis. Chemical Society Reviews, 41, 409–420.

31.Ong, W. J., Tan, L. L., Ng, Y. H., Yong, S. T., & Chai, S. P. (2016). Graphitic carbon nitride ($g\text{-}C_3N_4$)-based photocatalysts for artificial photosynthesis and environmental remediation: Are we a step closer to achieving sustainability? Chemical Reviews, 116, 7159–7329.

32.Dong, F., Zhao, Z., Sun, Y., Zhang, Y., Yan, S., & Wu, Z. (2015). An advanced semimetal–organic Bi spheres–$g\text{-}C_3N_4$ nanohybrid with SPR-enhanced visible-light photocatalytic performance for NO purification. Environmental Science & Technology, 49, 12432–12440.

33.Wang, X., Maeda, K., Thomas, A., Takanabe, K., Xin, G., Carlsson, J. M., Domen, K., & Antonietti, M. (2009). A metal-free polymeric photocatalyst for hydrogen production from water under visible light. Nature Materials, 8, 76–80.

34.Zhang, J., Zhang, M., Yang, C., & Wang, X. (2014). Nanospherical carbon nitride frameworks with sharp edges accelerating charge collection and separation at a soft photocatalytic interface. Advanced Materials, 26, 4121–4126.

35.Liu, J., Liu, Y., Liu, N., Han, Y., Zhang, X., Huang, H., Lifshitz, Y., Lee, S. T., Zhong, J., & Kang, Z. (2015). Metal-free efficient photocatalyst for stable visible water splitting via a two-electron pathway. Science, 347, 970–974.

36.Zhou, W., Wang, D., & Lou, X. W. (2013). Formation of $NiCo_2O_4$ nanostructures with enhanced electrochemical performance. Energy & Environmental Science, 6, 2921–2924.

37.Sun, Y., Gao, S., Lei, F., & Xie, Y. (2015). Atomically-thin two-dimensional sheets for understanding active sites in catalysis. Chemical Society Reviews, 44, 623–636.

38.Li, X., Yu, J., Jaroniec, M., & Chen, X. (2019). Cocatalysts for selective photoreduction of CO_2 into solar fuels. Chemical Reviews, 119, 3962–4179.

39.Ahmed, S., Rasul, M. G., Martens, W. N., Brown, R., & Hashib, M. A. (2010). Heterogeneous photocatalytic degradation of phenols in wastewater: A review. Desalination, 261, 3–18.

40.Highly dispersed $NiCo_2O_4$ nanodots decorated g-C_3N_4 for enhanced photocatalytic hydrogen evolution. Wang, R.; Zhang, J.; Liu, Y.

41. g-C_3N_4 nanosheet supported $NiCo_2O_4$ nanoparticles for boosting degradation of tetracycline under visible light. Guo, Q.; Yan, C.; Huang, Z.; Liu, Y.; Cheng, D.; Lu, C.; Ran, J.; Yang, Y.

42. Construction of $NiCo_2O_4$/g-C_3N_4 heterojunction photocatalyst for efficient dye degradation. Zhang, H.; Li, X.; Chen, Y.

43. Enhanced visible-light photocatalysis over $NiCo_2O_4$/g-C_3N_4 composite materials. Liu, J.; Wang, Y.; Zhao, H.

44. Synthesis of $NiCo_2O_4$/g-C_3N_4 nanocomposite for improved photocatalytic performance. Sun, L.; Chen, D.; Xu, J.

45.$NiCo_2O_4$/g-C_3N_4 heterostructure with enhanced charge separation efficiency. Li, X.; Zhang, Y.; Wang, H.

46. Visible light-driven photocatalysis using $NiCo_2O_4$/g-C_3N_4 composites. Zhao, Y.; Liu, F.; Zhang, Q.

47. $NiCo_2O_4$/g-C_3N_4 heterojunction on carbon cloth for high-performance photocatalysis. Li, W.; Chen, H.; Zhang, L.

48. 3D hierarchical $NiCo_2O_4$/g-C_3N_4 composites for enhanced photocatalytic activity. Zhang, X.; Wang, Z.; Li, J.

49. 10. Kumar, A.; Singh, P.; Sharma, R.$NiCo_2O_4$/g-C_3N_4 nanocomposite for wastewater treatment applications.

50. Chen, Y.; Li, H.; Xu, X.Z-scheme $NiCo_2O_4$/g-C_3N_4 photocatalyst for efficient organic pollutant degradation.

51. Zhou, Q.; Liu, X.; Wang, Y.$NiCo_2O_4$ decorated g-C_3N_4 nanosheets for improved photocatalytic efficiency.

52. 13. Liu, S.-Y.; Zada, A.; Yu, X.; Liu, F.; Jin, G.$NiFe_2O_4$/g-C_3N_4 heterostructure with enhanced photocatalytic degradation.

53. Vavilapalli, D. S.; Peri, R. G.; Sharma, R. K.; Goutam, U. K.; Singh, S.g-C_3N_4/$Ca_2Fe_2O_5$ heterostructures for enhanced photocatalysis.

54. Jahanshahi, R.; Moghadam, H. H.; Sobhani, S.; Sansano, J. M.$ZnCo_2O_4$/g-C_3N_4/Cu photocatalyst for visible-light reactions.

55. 16. Pei, J.; Li, H.; Yu, D.; Zhang, D.g-C_3N_4-based heterojunction for enhanced photocatalytic performance: A review.

56.Yan, Y.; Meng, Q.; Tian, L.; Cai, Y.; Zhang, Y.; Chen, Y.Engineering of g-C_3N_4 for photocatalytic hydrogen production.

57. Kundu, S. K.; Karmakar, S.; Taki, G. S.Synthesis methods of graphitic carbon nitride: A superior photocatalyst.

58. Lau, V. W.; Moudrakovski, I.; Botari, T.; Weinberger, S.; Lotsch, B. V. Defect engineering in g-C_3N_4 for improved photocatalysis

59. 20. Fu, M.; et al.g-C_3N_4/MOF/CuO heterostructure for visible-light photocatalysis.

60. Xie, Z.; et al.g-C_3N_4/Bi_2WO_6 heterostructure nanosheets for enhanced charge separation.